

# MSNet: A Deep Multi-scale Submanifold Network for Visual Classification

Ziheng Chen, Xiao-Jun Wu, Tianyang Xu, Rui Wang, Zhiwu Huang, and Josef Kittler

**Abstract**—The Symmetric Positive Definite (SPD) matrix has received wide attention as a tool for visual data representation in computer vision. Although there are many different attempts to develop effective deep architectures for data processing on the Riemannian manifold of SPD matrices, a very few solutions explicitly mine the local geometrical information in deep SPD feature representations. While CNNs have demonstrated the potential of hierarchical local pattern extraction even for SPD represented data, we argue that it is of utmost importance to ensure the preservation of local geometric information in the SPD networks. Accordingly, in this work we propose an SPD network designed with this objective in mind. In particular, we propose an architecture, referred to as MSNet, which fuses geometrical multi-scale information. We first analyse the convolution operator commonly used for mapping the local information in Euclidean deep networks from the perspective of a higher level of abstraction afforded by the Category Theory. Based on this analysis, we postulate a submanifold selection principle to guide the design of our MSNet. In particular, we use it to design a submanifold fusion block to take advantage of the rich local geometry encoded in the network layers. The experiments involving multiple visual tasks show that our algorithm outperforms most Riemannian SOTA competitors.

## I. INTRODUCTION

With the rapidly growing volume of media data, visual content recognition is attracting increasing attention in the computer vision and pattern recognition community. In this context, a surge of methods addressing this problem [1], [2], [3], [4], [5], [6], [7] attempt to use set-based methods to deal with visual classification, since a video sequence can be viewed as an image set [8], [9], [10], [11], [12], [13], [14], [15], [16], [17], [18],

Z. Chen, X.-J. Wu, T. Xu, and R. Wang are with the School of Artificial Intelligence and Computer Science, Jiangnan University, Wuxi, China. (e-mail: zh\_chen@stu.jiangnan.edu.cn, wu\_xiaojun@jiangnan.edu.cn, tianyang.xu@jiangnan.edu.cn, cs\_wr@jiangnan.edu.cn,).

Z. Huang is with the School of Computing and Information Systems, Singapore Management University, Singapore. (e-mail: zwhuang@smu.edu.sg).

J. Kittler is with the Centre for Vision, Speech and Signal Processing, University of Surrey, Guildford, GU2 7XH, UK. (e-mail: j.kittler@surrey.ac.uk).

[19]. Different from a single image, image sets contain more spatio-temporal appearance information about the content of interest. However, large within-set diversity and between-set similarity pose great challenges for accurate image set classification.

With their powerful capacity to model data variations, Symmetric Positive Definite (SPD) matrices have been shown to be successful in tackling this challenge. A series of powerful statistical representations can be constructed by SPD matrices for images and videos, including image set covariance matrices [20], [21], region covariance matrices [22], block-diagonal covariance descriptors [23] to name a few. However the non-Euclidean nature of SPD matrices precludes the use of the wide range of data analysis tools the applicability of which is confined to Euclidean metric spaces. Motivated by this problem, a number of Riemannian metrics have been introduced, such as Log-Euclidean metric (LEM) [24], Burg matrix divergence [25], Affine-Invariant Riemannian metric (AIM) [26], Stein divergence [27], and alpha-beta divergence [28]. With these well-studied Riemannian metrics, some Euclidean techniques can be generalized into the SPD manifold.

Some of these approaches attempt to learn a tangent map via logarithms of SPD matrices [21], or map the original SPD matrices into Reproducing Kernel Hilbert Spaces (RKHS) [20], [29], [30], [3]. However, these methods tend to distort the geometrical structure communicated by the data, since they model the manifold indirectly. To address this issue, [6], [5] suggest that a Riemannian mapping between manifolds aimed to obtain a lower-dimensional yet more discriminative manifold should be learnt directly. In addition, inspired by the significant progress achieved by deep learning [31], [32], [33], [34], [35], [36] attempt to build deep Riemannian networks for non-linear representation learning on SPD matrices.

Nevertheless, many existing deep Riemannian methods treat the SPD features as a global representation. Even if [34] attempts to mine the local information from SPD manifold, it fails to exploit the local geometrical cues. Given the success of multi-scale feature in both conventional feature design [37], [38] and deep learning

[39], [32], it should be promising to investigate its relevance for capturing statistically fine-grained information encoded in multi-scale SPD submanifolds. Accordingly, in this paper, we develop a deep multi-scale submanifold network designed to capture the informative local geometry when building a nonlinear model using a deep SPD network. To the best of our knowledge, this is the first work to successfully mine the local geometric information on the SPD matrices.

As convolution is the most successful technique dealing with local information in traditional convolutional neural networks (CNNs), we first analyze its mathematical essence from the perspective of the Category Theory, so as to identify the universal property which is able to explain the underlying mechanism of our proposed submanifold block designed to retain the local geometrical information. We employ SPDNet [33] as our backbone to extract compact low dimensional SPD representations. The proposed multi-scale submanifold block is thereby exploited to extract submanifolds of diverse sizes, each of which contains statistical information at a certain granularity level. This block captures not only holistic but also local geometry information, enriching the statistical information as is being concentrated by the network. Finally, we fuse the information in all these submanifolds in an appropriate space, which is essentially a diffeomorphic space, to aggregate the geometrical information at different scales.

In summary, our contribution is two-fold:

- A theoretical guideline is developed for the task of mining local information encoded in multi-scale submanifolds, based on the analysis of the Euclidean convolution from the perspective of the Category Theory.
- A novel multi-scale submanifold block is proposed to capture the local statistical information under the guidance of our theoretical analysis. This defines a new formulation of the image dataset classification problem, capable of preserving and encoding the geometric information in submanifolds, thus enhancing the representational capacity of the Riemannian deep learning.

The rest of the paper is organized as follows. We first discuss related work on SPD deep learning. The preliminary background is introduced next. We then proceed to describe our MSNet in detail. We evaluate the proposed method, and compare it with other Riemannian learning approaches on multiple datasets, showing its superiority.

## II. RELATED WORK

In order to take advantage of deep learning techniques, some effort has been made to generalize the Euclidean deep learning into a Riemannian one. For example, Huang and Van Gool [33] design a procedure involving a slice of spectral layers and backpropagation on the Riemannian matrix to obtain deep geometric feature maps. In their approach, bilinear mapping is exploited to simulate densely connected layer. Chakraborty *et al.*, [40] propose a theoretical framework for developing deep neural networks for manifold-valued data, exploiting the weighted Fréchet Mean to enable a convolution operation on a manifold. When applied to the SPD manifold, it models each frame by an SPD matrix and calculates the weighted Fréchet Mean of adjacent frames, attempting to simulate the 1D convolution in the temporal domain. However, different from Euclidean convolution, none of these methods pay attention to the local information in the SPD matrices. In contrast, Zhang *et al.*, [34] proposed an SPD transformation network for action recognition, where they design an SPD convolutional layer with the guarantee that the positive definiteness is preserved. The convolutional layer they designed is similar to the Euclidean convolution, except that the convolutional kernel is required to be SPD. Note that square matrices covered by a sliding window might not be SPD. Therefore, local geometry might be distorted or omitted, undermining the efficacy of their proposed network. In contrast, in our approach, the proposed mechanisms preserve the local information conveyed by submanifolds, by virtue of a novel multi-scale representation, which captures different levels of statistical information. The comprehensive statistical information, extracted in this way, facilitates visual classification.

## III. PRELIMINARIES

In order to develop our proposed method in Section IV, we first present the essential notions of Riemannian geometry of the SPD manifold, covariance descriptor and Category Theory. This will be followed by a brief introduction to basic SPDNet [33] layers.

### A. SPD Geometry

A  $d \times d$  real SPD  $S$  is denoted as  $S \in \mathcal{S}_{++}^d$  and  $\mathcal{S}^d$  denotes  $d \times d$  real symmetric matrices. Then  $S \in \mathcal{S}_{++}^d$  iff for all non-zero vector  $v \in \mathbb{R}^d$ ,  $v^T S v > 0$ . We denote  $\log(\cdot) : \mathcal{S}_{++}^d \rightarrow \mathcal{S}^d$  as matrix logarithm and  $T_S \mathcal{M}$  as the tangent space of the manifold  $\mathcal{M}$  at the point  $S \in \mathcal{S}_{++}^d$ . As studied by Arsigny *et al.*, [41],  $\mathcal{S}_{++}^d$  is diffeomorphic by matrix logarithm  $\log(\cdot)$  to the tangent space  $T_I \mathcal{M}$  at the identity, *i.e.*,  $\mathcal{S}^d$ .

### B. Covariance Descriptor

The covariance descriptor, a widely used statistical representation for visual data, encodes correlation of the samples. For a given image set  $X$ , its covariance can be computed as follows,

$$C = \frac{1}{n-1} X H_d X^T, \quad (1)$$

where the mean vector of  $X$ , namely  $\mu$ , is implicitly computed by the centring matrix  $H_d = I_d - \frac{1}{n} \mathbf{1}_d \mathbf{1}_d^T$ . As studied in [26], the covariance matrix lies on an SPD manifold  $\mathcal{S}_{++}^d$  associated with

$$S = C + \lambda \operatorname{tr}(C) I_d. \quad (2)$$

In the following, we set  $\lambda = 1e^{-3}$ .

### C. Foundations of the Category Theory

The Category Theory studies the universal properties and mathematical abstractions shared by different domains, similar to the object-oriented programming in computer science. A category is defined in Definition 1.

*Definition 1:* A category  $\mathcal{C}$  is:

- A collection of objects, denoted by  $\operatorname{Obj}(\mathcal{C})$ .
- For any two objects  $A, B \in \operatorname{Obj}(\mathcal{C})$ , collections of morphisms between them is denoted by  $\operatorname{Hom}(A, B)$ . (The collection of all morphisms in  $\mathcal{C}$  is denoted by  $\operatorname{Mor}(\mathcal{C})$  )

Let us take the linear space, which is widely studied in pattern recognition, as an example. In this category, the objects are linear spaces and morphisms are linear homomorphisms. Besides, morphisms in Definition 1 should satisfy several axioms, like composition, associativity and identity. Please refer to the discussions [42] for comprehensive understanding.

The Category Theory enables us to develop a mathematical abstraction of operations in one category and generalize them into another category. In our approach, the Category Theory suggests that the convolution effectively captures the local linear information in a Euclidean space and then transfers this knowledge to a class of SPD manifolds. This construct provides a useful template for the design of our submanifold block in Section IV.

### D. Operations on the SPDNet

By analogy to the conventional fully connected networks, Huang and Van Gool [33] proposed an SPDNet to perform deep learning that respects the SPD manifold. Let  $S_{k-1} \in \mathcal{S}_{++}^d$  be the input SPD matrix to the  $k^{th}$  layer. We differentiate between the following SPD layers:

- BiMap layer: This layer is designed to transform the input SPD matrices to compact and discriminative

SPD matrices by  $S_k = W_k S_{k-1} W_k^T$ . To guarantee the output to be SPD, the transformation matrix  $W_k$  is constrained to be semi-orthogonal.

- ReEig layer: This layer serves as an activation function like RELU in a conventional deep network. It is responsible for introducing non-linearity into SPDNet. It is defined as follows:  $S_k = U_{k-1} \max(\epsilon I, \Sigma_{k-1}) U_{k-1}^T$ , where  $\epsilon > 0$  is a threshold and  $U_{k-1}, \Sigma_{k-1}$  define the eigenvalues decomposition,  $S_{k-1} = U_{k-1} \Sigma_{k-1} U_{k-1}^T$ .
- LogEig layer: This layer aims to map the SPD manifold into a Euclidean space. In this way, a Euclidean loss function can be used. This layer is defined by matrix logarithm:  $S_k = U_{k-1} \log(\Sigma_{k-1}) U_{k-1}^T$ . The LogEig layer, together with fully connected layer, softmax and cross entropy, are used to solve classification tasks with SPD representations.

## IV. PROPOSED METHOD

Analogous to the successful convolutional neural network, the proposed network is designed to capture multi-scale local information in the category of Riemannian manifold. Specifically, we first apply SPDNet as our backbone to obtain a low-dimensional discriminative SPD manifold. Then we extract submanifolds at diverse granularity levels and fuse these local sources of information for regular output layers via the proposed multi-scale submanifold block. The proposed network is conceptually illustrated in Fig. 1. As convolution is the most successful technique to deal with local information in the deep learning paradigm, it is important to analyze its mathematical essence and transfer its key points into the SPD manifold. To this end, in the next subsection, we first analyze the Euclidean space convolution from the perspective of the Category Theory to shed light on the design of our multi-scale submanifold block. Then we describe our innovative multi-scale submanifold block.

### A. Analysis of Euclidean Convolution

Since the convolution is an operation in the category of linear space, we first consider it from the perspective of linear algebra. Then we will proceed with the analysis via the Category Theory to derive the general properties that can be transferred into the SPD manifold.

To avoid tedious subscripts, we consider an example whose input and output are single channel tensors. In this case, only one kernel filter is involved, but the following analysis can also be generalized into an arbitrary number of channels readily. In convolution networks, the tensor feature and the  $i^{th}$  receptive field can be viewed as the linear space  $V$  and subspace  $V_i$ , respectively. The process

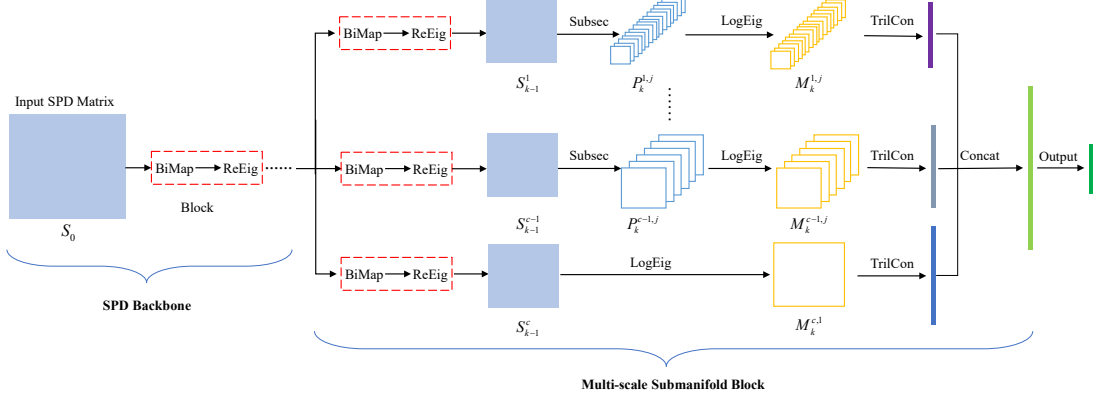


Fig. 1: Illustration of the proposed Multi-scale Submanifold Network (MSNet). We first employ SPDNet [33] as our backbone to extract lower dimensional, yet more discriminative SPD feature representations. Then in each branch, a BiMap-ReEig block is exploited to obtain an SPD representation  $S_{k-1}^i$ , where  $k-1$  and  $i$  are layer and channel index respectively. We propose a submatrix selection, denoted as SubSec, to result in  $P_k^{i,1} \dots P_k^{i,n^i}$  along the  $i^{th}$  channel for local manifold feature learning, where  $n^i$  is the number of selected submanifolds in the  $i^{th}$  channel. Next, LogEig layer is applied to map each submatrix feature into a Euclidean space, *i.e.*,  $M_k^{i,j} = \log(P_k^{i,j})$ . Finally, we apply TrilCan to go through a process of extracting a lower triangular matrix, vectorization and concatenation. Finally, we concatenate all the vectors from the different branches with a Concat layer, followed by any regular output layers like softmax layer. Note that the SPD matrix itself can also be viewed as a trivial submanifold, encoding global information, and hence the bottom branch is exploited to capture global information, which is how SPDNet works.

that the  $i^{th}$  receptive field is reduced into a real scalar by a specific kernel filter can be deemed as a linear mapping  $f_i : V_i \rightarrow M_i$ . Note that  $M_i$  is a trivial one dimensional linear space,  $\mathbb{R}$ . After convolution, each receptive field is reduced into a real number and these scalar elements are concatenated to build a new tensor feature. This process can be more generally described by the notion of direct sum “ $\oplus$ ” [43] in linear algebra, *i.e.*,  $M = M_1 \oplus \dots \oplus M_n$ . Note that the direct sum, “ $\oplus$ ”, which is an operation that builds a new linear space from two subspaces, can be intuitively understood as a counterpart of the union in the set theory. The above analysis leads to the following abstraction of the convolution operation.

*Proposition 1:* (Convolution) For a given linear space  $V$  of dimension  $d \times d$ ,  $n$  linear subspaces  $V_1, V_2, \dots, V_n$  of dimension  $k \times k$  are selected and a linear function  $f_i(\cdot) : V_i \rightarrow M_i$  is performed in each of them to extract local linear information. The resulting linear spaces  $M_1, \dots, M_n$  are combined into a final linear space  $M$  by direct sum, *i.e.*,  $M = M_1 \oplus \dots \oplus M_n$ .

To discover more general property of Euclidean convolution, we further analyze it by the Category Theory. To this end, we can simply substitute the linear algebra terms with category language following the axioms of the Category Theory. In detail, linear space  $V$ , subspace  $V_i$  and linear function  $f_i$  can be more generally described as object  $A$ , sub-object  $A_i$  and morphism  $f_i$ . Besides,

we notice that each subspace  $V_i$  shares the same dimensionality, which indicates  $V_1, \dots, V_n$  are equivalent in the sense of linear space. This suggests that the extracted sub-objects  $A_1, \dots, A_n$  should be isomorphic. However, not all categories share the idea of direct sum. For example, the categories, known as group, ring and field, do not have this kind of operation. Therefore, the combination strategies vary in different categories. Now, we could obtain a more general description of convolution by the Category Theory.

*Proposition 2:* (Convolution) In a category  $\mathcal{C}$ , for an object  $A \in Obj(\mathcal{C})$ , we extract  $n$  isomorphic sub-objects from  $A$ , denoted by  $A_1, A_2, \dots, A_n$ . Then morphism  $f_i \in Hom(A_i, B_i)$  is applied to each sub-object to map it into a resulting object  $B_i$ . The resulting objects  $B_1, \dots, B_i$  are combined into a final object  $B \in Obj(\mathcal{C})$  according to certain principles.

With the Proposition 2 as an intermediary, we can generalize the convolution into the Riemannian manifold theoretically. Specifically, the object, sub-object and morphism in Riemannian manifold is manifold, submanifold and Riemannian mapping respectively.

*Proposition 3:* (Convolution) For a Riemannian manifold  $\mathcal{M}$ , we extract  $n$  isomorphic submanifolds  $\mathcal{M}_1, \mathcal{M}_2, \dots, \mathcal{M}_n$  and map each one of them by a Riemannian mapping  $f_i(\cdot) : \mathcal{M}_i \rightarrow \mathcal{M}'_i$ . The resulting manifolds  $\mathcal{M}'_i$  are aggregated into a final manifold  $\mathcal{M}'$  according to a certain principles.

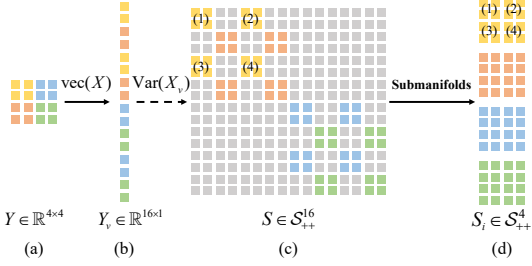


Fig. 2: Illustration of the process of selecting principal submatrices. (a) We deem an  $S \in \mathcal{S}_{++}^{16}$  as a covariance matrix from an imaginary  $4 \times 4$  random matrix  $Y$ . We use a  $2 \times 2$  sliding window with skip of 2 on  $X$  to obtain the corresponding position index. We use four kinds of colour to denote the four regions of interest. (b) shows the corresponding indexes of the four region in vectorized  $Y_v$ . (c) Then we can find the corresponding region covariance matrices for the four regions from  $S$ . (d) The region covariance matrices  $S_i \in \mathcal{S}_{++}^4$  corresponding to these local regions are the submanifolds we select.

As a summary of the above discussion, we obtain two important insights about convolution, helping the design of our submanifold block. Firstly, not all sub-objects are involved, and all the selected sub-objects should be isomorphic. Secondly, a specific way of aggregating sub-objects should be elaborately designed according to the axioms of the category.

### B. Multi-scale Submanifold Block

In view of the above analysis, there are two factors we should consider when designing our submanifold block, *i.e.*, the rule for selecting isomorphic submanifolds and the way of aggregating them. In the following, we first discuss the details of selecting submanifolds in the SPD manifold. Then we proceed to introduce our multi-scale submanifold block, which fuses submanifolds via a divide-aggregation strategy.

1) *The Principles for Selecting Submanifolds*: One thing that needs clarifying is that the isomorphic submanifolds in SPD manifold are the principal submatrices of the same size. Note that incorporating all the sub-objects might not be an optimal solution, since it introduces redundant information with cumbersome computation. In conventional convolution, sub-objects are selected following the concept of receptive field. In terms of a specific SPD manifold, the number of principal submatrices grows combinatorially, which could cause dimensionality explosion. For instance, if we select all the principal submatrices of  $4 \times 4$  from a  $16 \times 16$  SPD matrix, which seems like a trivial example, the total number of selected submatrices would be  $C_{16}^4 = 1820$ . In most cases, this huge number of small SPD submatrices

would not be manageable, even in this relatively easy case, let alone when dealing with real-world data in the SPD deep network. Therefore, it is crucial to select principal submatrices to construct submanifolds. Based on the conclusion of this analysis, we introduce a method of selecting principal submatrices of the same size from the SPD feature.

In probability theory, the distribution information of a  $d \times d$  random matrix  $X$  can be conveyed by its covariance matrix  $S$  of  $d^2 \times d^2$ , where  $S = \text{Var}(\text{vec}(X))$  and  $\text{vec}(\cdot)$  denotes vectorization. The covariance of a  $k \times k$  local region in  $X$  corresponds to a  $k^2 \times k^2$  principal submatrix of  $S$ . If we focus on multiple  $k \times k$  local regions, we then can extract a series of principal submatrices of  $k^2 \times k^2$ , which is isomorphic. Considering that an SPD matrix is often defined by covariance in computer vision, we can follow this probabilistic clue to select principal submatrices.

Specifically, according to statistics, for a given image set consisting of images  $X_1, \dots, X_m$  of the size  $n \times n$ , it can be viewed as  $m$  samples from a population, an  $n \times n$  random matrix  $X$ . Then we estimate population covariance by sample covariance and model it into an  $n^2 \times n^2$  SPD matrix  $S_0$  by Eqs. (1) and (2). After forward passing the deep SPD networks, we obtain a lower-dimensional discriminative SPD matrix  $S$  of  $d^2 \times d^2$  via the network mapping denoted by  $\phi(\cdot) : \mathcal{S}_{++}^{n^2} \rightarrow \mathcal{S}_{++}^{d^2}$ . We hypothesize that there is an implicit mapping  $\psi(\cdot) : \mathbb{R}^{n \times n} \rightarrow \mathbb{R}^{d \times d}$  to transform the random matrix  $X$  into another one  $\psi(X)$  and  $S$  is the covariance of  $\psi(X)$ . We denote  $\psi(X)$  as  $Y$  for simplicity and then the size of  $Y$  is  $d \times d$ . If we focus on the local region covariance of  $Y$ , then we can extract a series of principal submatrices from  $S$ . Besides, the number of submatrices extracted in this way is much smaller than combinatorial number.

More specifically, we view a  $d^2 \times d^2$  SPD matrix  $S$  as a covariance from a  $d \times d$  random matrix  $Y$ . The covariance matrix associated with a  $k \times k$  receptive field of the imaginary matrix  $Y$  corresponds to a  $k^2 \times k^2$  principal submatrix of  $S$ . When moving a  $k \times k$  sliding window by a step equal to  $s$  in  $Y$  (to obtain the position index), we can select  $(\frac{d-k}{s} + 1)^2$  principal submatrices of  $S$  accordingly. Obviously, the submatrices we select are still SPD and the number of them is much smaller than  $C_{d^2}^{k^2}$ . Besides, it will encode the geometrical information conveyed by the local system in the category of SPD manifold. Fig. 2 provides a conceptual illustration of the process of selecting submanifolds.

2) *Multi-scale Mechanism*: In fact, in deep SPD network, hidden SPD feature contains statistically compact information. Each element of the hidden feature reflects the region correlation in original video. By extracting

principal submatrices, we focus on correlation among multiple local regions. In this way, we can capture the local semantic information in a statistical form. We anticipate that the classification can benefit from this compact local statistical information.

Furthermore, inspired by Res2Net [44], which attempts to capture multi-scale feature in one single residual block, we design a multi-channel mechanism to obtain local manifold information at diverse granularity levels. In detail, for an SPD feature, various BiMap-ReEig layers are applied to obtain a low dimensional SPD matrix, by:

$$\begin{aligned} S_{k-1}^i &= W_{k-1}^i S_{k-2} W_{k-1}^{iT}, \\ S_k^i &= U_{k-1}^i \max(\epsilon I, \Sigma_{k-1}^i) U_{k-1}^{iT}, \end{aligned} \quad (3)$$

where all  $W_{k-1}^i$  are of the same size.

It is expected that in each channel, the primary local geometrical information  $S_k^i$  learnt during training varies. To capture it, submatrices with specific  $k_i \times k_i$  dimensions are extracted from  $S_k^i$ . In this way, rich statistical local information at different granularity levels is extracted by our network. Besides, as an SPD matrix itself can be viewed as a trivial submanifold, we also incorporate a channel capturing the global information. In this way, not only the holistic geometry, but also local geometry are jointly captured in the category of SPD manifold.

3) *Submanifolds Fusion Strategies*: If we follow the Proposition 3 rigorously, it would result in a major computational burden, in view of the complex structure of Riemannian manifold. Therefore, we fuse this multi-scale information in an approximate way instead. Since the  $\mathcal{S}_{++}^d$  is diffeomorphic to  $\mathcal{S}^d$  by matrix logarithm and  $\mathcal{S}^d$  forms a Euclidean space, we can fuse the multi-scale information in a comparatively simple space, *i.e.*,  $\mathcal{S}^d$ , which is a well known technique for tackling the problems of data analysis on SPD manifold [21].

To be more specific, we first map each principal submatrix into a real symmetric matrix by matrix logarithm,  $M_k^{ij} = \log(P_k^{ij})$ , where  $k, i$  and  $j$  represent  $k^{th}$  layer,  $i^{th}$  channel, and  $j^{th}$  submatrix respectively. Considering that the dimensionality of the Euclidean space formed by symmetric matrices  $\mathcal{S}^d$  is  $\frac{d(d+1)}{2}$ , for each  $M_k^{ij}$ , we exploit its lower triangular part to further mitigate the computational burden. Since at this point the features lie in a Euclidean space, concatenation can be applied to fuse them. This process can be formally described as:

$$V_k^i = \text{concat}(\text{vec}(\text{tril}(M_k^{i1})), \dots, \text{vec}(\text{tril}(M_k^{in^i}))) \quad (4)$$

where  $\text{vec}(\cdot)$  means vectorization.

After we fuse the local information in each channel, we concatenate the feature vectors to aggregate the multi-scale information in different channels.

## V. EXPERIMENTS

We evaluate the proposed MSNet in three challenging visual classification tasks: video-based action recognition with the Cambridge-Gesture (CG) [45] and the UCF-101 [46] datasets, and skeleton-based action recognition with the First-Person Hand Action (FPHA) [47] dataset, respectively. We simply employ fully connected layer, softmax layer and cross entropy as our output layer as [33], [48]. For training our MSNet, we use an i5-9400 (2.90GHz) CPU with 8GB RAM.

### A. Implementation Details

The SOTA Riemannian learning competitors include: 1). *General methods for SPD learning*: Covariance Discriminative Learning (CDL) [3], SPD Manifold Learning (SPDML-AIM, SPDML-Stein) [6] and Log-Euclidean Metric Learning (LEML) [21]; 2). *General methods for Grassmann learning*: Grassmann Discriminant Analysis (GDA) [2] and Projection Metric Learning (PML) [49]; 3). *Hybrid Riemannian manifold learning methods*: Hybrid Euclidean-and-Riemannian Metric Learning (HERML) [7] and Multiple Manifolds Metric Learning (MMML) [4]; 4). *Riemannian deep methods*: SPD Network (SPDNet) [33], SymNet [35], Grassmannian Network (GrNet) [48]. All the comparative methods are carefully re-implemented by the source codes and fine-tuned according to the original papers.

To further evaluate the effectiveness of our algorithm, we also compare our MSNet with conventional SOTA hand pose estimation methods on the FPHA dataset. These approaches include Lie Group [50], Hierarchical Recurrent Neural Network (HBRNN) [51], Jointly Learning Heterogeneous Features (JOULE) [52], Convolutional Two-Stream Network (Two stream) [53], Novel View [54], Transition Forests (TF) [55], Temporal Convolutional Network (TCN) [56], LSTM [47] and Unified Hand and Object Model [57]. Besides, we also compare our approach against Euclidean network searching methods, DARTS [58] and FairDARTS [59], following the setting in [60] by viewing SPD logarithm maps as Euclidean data.

We study five configurations, *i.e.*, MSNet-H, MSNet-PS, MSNet-AS, MSNet-S and MSNet-MS to further evaluate the utility of our proposed network. In detail, MSNet-MS with two BiMap-ReEig layers is  $S_0 \rightarrow f_b^{(1)} \rightarrow f_r^{(2)} \rightarrow f_b^{(3)} \rightarrow f_r^{(4)} \rightarrow f_m^{(5)} \rightarrow f_f^{(6)}$   $\rightarrow$

Dataset	BiMap Setting	Submanifolds	$\epsilon$	Epochs
CG	$\{100, 80, 50, 25\}$	$\{2^2, 3^2, 4^2, 5^2\}$	$1e^{-5}$	500
FPHA	$\{63, 56, 46, 36\}$	$\{5^2, 6^2\}$	$1e^{-4}$	3500
UCF-sub	$\{100, 80, 49\}$	$\{2^2, 6^2, 7^2\}$	$1e^{-5}$	500

TABLE I: Configuration of MSNet on three datasets. Note that  $\{100, 80, 50, 25\}$  means  $100 \times 80, 80 \times 50, 50 \times 25$ .

$f_s^{(7)}$ , where  $f_b^{(k)}, f_r^{(k)}, f_m^{(k)}, f_f^{(k)}, f_s^{(k)}$  represent  $k^{th}$  layers of BiMap, ReEig, multi-scale submanifold, FC, and softmax-cross-entropy, respectively. Note that apart from the two BiMap-ReEig blocks in the backbone, in each branch of  $f_m^{(k)}$ , there is a BiMap-ReEig block as well, as illustrated in Fig. 1. Besides, as the whole SPD matrix can be viewed as a trivial submanifold, we use MSNet-H to denote that we only extract holistic information. Though it is similar with SPDNet, only lower triangular part is exploited for classification in our framework, alleviating the computational burden. To study the utility of proper submanifolds, we use MSNet-PS to represent that we extract all kinds of proper submanifolds according to our principles except the trivial one. To see whether over-loaded submanifolds would bring about redundant information, we build MSNet-AS to extract all the submanifolds including the trivial one. MSNet-S denotes that we only utilize the proper submanifolds in the corresponding MSNet-MS except the trivial one.

In the experiments, we simply set “step” size equal to 1. The above models of our MSNet and SPDNet share the same learning mechanism as follows. The initial learning rate is  $\lambda = 1e^{-2}$  and reduced by 0.8 every 50 epochs to a minimum of  $1e^{-3}$ . Besides, the batch size is set to 30, and the weights in BiMap layers are initialized as random semi-orthogonal matrices. For activation threshold in ReEig and dimension of transformation matrices in BiMap, we first search the optimal settings by our backbone SPDNet and then employ the same settings to our MSNet.

### B. Datasets and Settings

To evaluate our method when facing limited data, experiments are carried out on the CG [45] dataset. It consists of 900 video sequences covering nine kinds of hand gesture. For this dataset, following the criteria in [61], we randomly select 20 and 80 clips for training and testing per class, respectively. For evaluation, we resize each frame into  $20 \times 20$  and obtain the grey scale feature. To further facilitate our experiment, we reduce each frame dimension into 100 by PCA. Then we compute the covariance matrix of size  $100 \times 100$  to represent each video.

Methods	Year	Color	Depth	Pose	Acc.
Lie Group [50]	2014	$\times$	$\times$	$\checkmark$	82.69
HBRNN [51]	2015	$\times$	$\times$	$\checkmark$	77.40
JOULE [52]	2015	$\checkmark$	$\checkmark$	$\checkmark$	78.78
Two stream [53]	2016	$\checkmark$	$\times$	$\times$	75.30
Novel View [54]	2016	$\times$	$\checkmark$	$\times$	69.21
TF [55]	2017	$\times$	$\times$	$\checkmark$	80.69
TCN [56]	2017	$\times$	$\times$	$\checkmark$	78.57
LSTM [47]	2018	$\times$	$\times$	$\checkmark$	80.14
H+O [57]	2019	$\checkmark$	$\times$	$\times$	82.43
DARTS [58]	2018	$\times$	$\times$	$\checkmark$	74.26
FairDARTS [59]	2020	$\times$	$\times$	$\checkmark$	76.87
SPDML-AIM [6]	2018	$\times$	$\times$	$\checkmark$	76.52
HERML [7]	2015	$\times$	$\times$	$\checkmark$	76.17
MMML [4]	2018	$\times$	$\times$	$\checkmark$	75.05
SPDNet [33]	2017	$\times$	$\times$	$\checkmark$	85.57
GrNet [48]	2018	$\times$	$\times$	$\checkmark$	77.57
SymNet [35]	2021	$\times$	$\times$	$\checkmark$	82.96
<b>MSNet-H</b>		$\times$	$\times$	$\checkmark$	85.74
<b>MSNet-PS</b>		$\times$	$\times$	$\checkmark$	80.52
<b>MSNet-AS</b>		$\times$	$\times$	$\checkmark$	82.26
<b>MSNet-S</b>		$\times$	$\times$	$\checkmark$	86.61
<b>MSNet-MS</b>		$\times$	$\times$	$\checkmark$	<b>87.13</b>

TABLE II: Recognition Results (%) on the FPHA Dataset. Best Results are Highlighted in **Bold**.

We employ the popular FPHA [47] dataset for skeleton-based action recognition. It includes 1,175 action videos of 45 different action categories. For a fair comparison, we follow the protocols in [35]. In detail, we use 600 action clips for training and 575 for testing and each frame is vectorized into a 63-dimensional feature vector with the provided 3D coordinates of 21 hand joints. Then we obtain a  $63 \times 63$  covariance representation for each sequence.

To assess the utility of our method in the task of relatively large scale, UCF-101 [46] dataset is exploited, which is sourced from YouTube, containing 13k realistic user-uploaded video clips of 101 types of action. To facilitate our experiment, 50 kinds of action are randomly selected, each of which consists of 100 clips. We call this dataset UCF-sub in the following. As what we did in the CG dataset, we exploit grey scale feature and reduce the dimension of each frame into 100 by PCA. The seventy-thirty-ratio (STR) protocol is exploited to build the gallery and probes.

The configurations on three datasets are listed in Tab. I.

### C. Analysis

As reported in Tab. II and Tab. III, our proposed MSNet-MS outperforms all the other competitors on

Method	CG	UCF-sub
GDA [2]	88.68	43.67
CDL [3]	90.56	41.53
PML [49]	84.32	50.60
LEML [21]	71.15	44.67
SPDML-Stein [6]	82.62	51.40
SPDML-AIM [6]	88.61	51.13
HERML [7]	88.94	NA
MMML [4]	89.92	NA
GrNet [48]	85.69	35.80
SPDNet [33]	89.03	59.93
SymNet [35]	89.81	56.73
MSNet-H	89.03	58.27
MSNet-PS	90.14	57.73
MSNet-AS	NA	58.33
MSNet-S	90.14	59.40
MSNet-MS	<b>91.25</b>	<b>60.87</b>

TABLE III: Recognition Results (%) on the CG and UCF-sub datasets. Best results are highlighted in **Bold**.

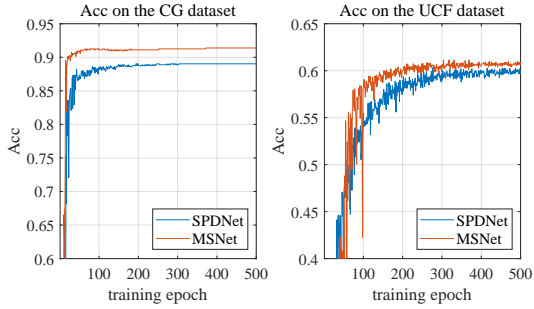


Fig. 3: Accuracy curve of the proposed MSNet against SPDNet on the CG and UCF-sub datasets.

three datasets. Note that in relatively large dataset, some shallow learning methods, such as MMML and HERML, is barely feasible in view of its time-consuming optimization. Fig. 3 shows the convergence behaviour on the CG and UCF-sub datasets. There are several interesting observations worth discussion.

Firstly, although hybrid Riemannian methods, like HERML and MMML, can take advantage of complementary information encoded in different manifold and thus surpass some deep methods occasionally, our method consistently outperforms them. This verifies that information encoded in submanifolds is of great importance and could be beneficial for classification.

Secondly, on the CG and FPHA datasets, MSNet-H achieves almost the same performance as SPDNet, while on the UCF-sub dataset, MSNet-H is inferior to SPDNet. Although as we discussed in Sec. IV-B1, lower triangular part of a symmetric matrix is mathematically equivalent to itself, the non-convexity of optimization on deep learning might cause some empirical deviation. However, extracting lower triangular, which is the way we exploit, could

alleviate the computational burden and thus enhance the scalability of the output layer. For instance, if a deep network is used as an output classifier, it would be more efficient to halve the dimensionality of the input vector. What's more, our method, *i.e.*, MSNet-MS, surpasses the backbone network, SPDNet, in all the three datasets. This suggests that the underlying statistical information in submanifolds could contribute to the visual perception, leading to a better classifier. Therefore, efforts should be paid to mine the information in submanifolds. However, over-saturated efforts in submanifolds might undermine the discriminability. This idea is justified by the generally inferior performance of MSNet-AS, which selects all the submanifolds, to MSNet-MS.

Thirdly, although proper efforts should be made for submanifolds, they might vary for different tasks. On the CG dataset, best performance is achieved when we use all kinds of submanifolds. This might be attributed to the particularity of the dataset. In detail, on this dataset, the background and the foreground are relatively monotonous, and the difference between them is apparent. Therefore, statistical information at diverse granular level encoded in different submanifolds could contribute to the classification. However, on the FPHA and UCF-sub datasets, the large variance of appearance makes us cautious to select submanifolds to waive the statistically dispensable information.

More importantly, although local statistical information is of great value for visual classification, never can we neglect the importance of holistic information. Specifically, as we can see, MSNet-MS is superior to MSNet-S. The sole difference between these two configurations is that MSNet-MS uses the global information, while MSNet-S does not. The consistent phenomenon can be observed in the comparison between MSNet-AS and MSNet-PS. This indicates that only when we combine the optimal local information together with global information, could we make the best of statistical information.

It takes about 1.29s, 2.67s and 34.50s per epoch to train our MSNet-MS on the CG, FPHA and UCF-sub datasets respectively, while training SPDNet takes 0.53s, 1.53s and 11.33s per epoch. Although the extra time caused by our multi-branch mechanism is inevitable, our method demonstrates the significance of submanifold for visual perception.

#### D. Ablation Study

To further evaluate the utility of our MSNet, different configurations, like depth and transformation matrices in SPD backbone, are implemented on the UCF-sub

Configuration	SPDNet	MSNet
{100,60,36}	56.73	57.33
{100,80,60,36}	56.27	58.33
{100,80,50,25}	48.47	52.67
{100,80,50,25,16}	40.07	45.60
{100,80,50,25,9}	28.73	36.07

TABLE IV: Performance (%) on the UCF-sub dataset under different backbone configurations.

dataset, as shown in Tab. IV. Apart from the expected consistent performance gain brought about by our submanifold block, there is another interesting observation. The magnitude of improvement varies under different configurations. To be more specific, in some configurations, like {100,60,36}, the improvement sourced from our MSNet is relatively marginal, while in other cases, our approach offers more incremental gain, especially in the case of {100,80,50,25,9}, where the SPDNet is highly underfitting. This indicates that by providing complementary geometrically local information, submanifold is not only beneficial for Riemannian deep learning and could alleviating underfitting. It is therefore expected that the study of submanifold is worthwhile in the sense of promoting Riemannian deep learning forward.

## VI. CONCLUSION

In this paper we have proposed a novel multi-scale submanifold network for visual classification. Extensive experiments demonstrate the superiority of our approach. To the best of our knowledge, this work is the first attempt to mine the diverse local geometry in the Riemannian deep network paradigm. It opens a new direction that mines the information in high-level semantic submanifold, that is beneficial for Riemannian deep learning.

However, there are still some issues to be improved. For instance, our manual principle for selection is a sub-optimal expedient. In the future, we will explore the feasibility of Riemannian feature selection and apply it to submanifold selection. Besides, applying neural architecture search [60] to determine the specific branches in multi-scale block might be another future avenue.

## REFERENCES

- [1] W. Wang, R. Wang, Z. Huang, S. Shan, and X. Chen, “Discriminant analysis on riemannian manifold of gaussian distributions for face recognition with image sets,” *CVPR*, pp. 2048–2057, 2015.
- [2] J. Hamm and D. D. Lee, “Grassmann discriminant analysis: a unifying view on subspace-based learning,” *ICML*, pp. 376–383, 2008.
- [3] R. Wang, H. Guo, L. S. Davis, and Q. Dai, “Covariance discriminative learning: A natural and efficient approach to image set classification,” *CVPR*, pp. 2496–2503, 2012.
- [4] R. Wang, X.-J. Wu, K.-X. Chen, and J. Kittler, “Multiple manifolds metric learning with application to image set classification,” *ICPR*, pp. 627–632, 2018.
- [5] Z. Gao, Y. Wu, M. Harandi, and Y. Jia, “A robust distance measure for similarity-based classification on the spd manifold,” *IEEE-TNNLS*, vol. 31, no. 9, pp. 3230–3244, 2019.
- [6] M. Harandi, M. Salzmann, and R. Hartley, “Dimensionality reduction on spd manifolds: The emergence of geometry-aware methods,” *IEEE-TPAMI*, vol. 40, no. 1, pp. 48–62, 2017.
- [7] Z. Huang, R. Wang, S. Shan, and X. Chen, “Face recognition on large-scale video in the wild with hybrid euclidean-and-riemannian metric learning,” *PR*, vol. 48, no. 10, pp. 3113–3124, 2015.
- [8] X. Luo, Z. Zhang, and X. Wu, “A novel algorithm of remote sensing image fusion based on shift-invariant shearlet transform and regional selection,” *AEU-International Journal of Electronics and Communications*, vol. 70, no. 2, pp. 186–197, 2016.
- [9] Y.-J. Zheng, J.-Y. Yang, J. Yang, X.-J. Wu, and Z. Jin, “Nearest neighbour line nonparametric discriminant analysis for feature extraction,” *Electronics Letters*, vol. 42, no. 12, pp. 679–680, 2006.
- [10] X. Luo, Z. Zhang, B. Zhang, and X.-J. Wu, “Image fusion with contextual statistical similarity and nonsubsampled shearlet transform,” *IEEE Sensors Journal*, vol. 17, no. 6, pp. 1760–1771, 2017.
- [11] T. Xu, Z.-H. Feng, X.-J. Wu, and J. Kittler, “Learning low-rank and sparse discriminative correlation filters for coarse-to-fine visual object tracking,” *IEEE Transactions on Circuits and Systems for Video Technology*, vol. 30, no. 10, pp. 3727–3739, 2019.
- [12] S.-G. Chen and X.-J. Wu, “A new fuzzy twin support vector machine for pattern classification,” *International Journal of Machine Learning and Cybernetics*, vol. 9, no. 9, pp. 1553–1564, 2018.
- [13] T. Xu, Z.-H. Feng, X.-J. Wu, and J. Kittler, “An accelerated correlation filter tracker,” *Pattern Recognition*, vol. 102, p. 107172, 2020.
- [14] C. Li, W. Yuan, A. Bovik, and X. Wu, “No-reference blur index using blur comparisons,” *Electronics letters*, vol. 47, no. 17, pp. 962–963, 2011.
- [15] T. Xu, Z. Feng, X.-J. Wu, and J. Kittler, “Adaptive channel selection for robust visual object tracking with discriminative correlation filters,” *International Journal of Computer Vision*, vol. 129, no. 5, pp. 1359–1375, 2021.
- [16] M. Wang, S. Wang, and X.-J. Wu, “Initial results on fuzzy morphological associative memories,” *Journal of Electronics*, vol. 31, no. 005, pp. 690–693, 2003.
- [17] J. Sun, W. Fang, and X.-J. Wu, “Quantum-behaved particle swarm optimization: principle and applications,” 2011.
- [18] J. Sun, C. Li, X.-J. Wu, V. Palade, and W. Fang, “An effective method of weld defect detection and classification based on machine vision,” *IEEE Transactions on Industrial Informatics*, vol. 15, no. 12, pp. 6322–6333, 2019.
- [19] H. Li, X.-J. Wu, and T. Durrani, “Nestfuse: An infrared and visible image fusion architecture based on nest connection and spatial/channel attention models,” *IEEE Transactions on Instrumentation and Measurement*, vol. 69, no. 12, pp. 9645–9656, 2020.
- [20] Z. Chen, T. Xu, X.-J. Wu, R. Wang, and J. Kittler, “Hybrid riemannian graph-embedding metric learning for image set classification,” *IEEE-TBD*, 2021.
- [21] Z. Huang, R. Wang, S. Shan, X. Li, and X. Chen, “Log-euclidean metric learning on symmetric positive definite manifold with application to image set classification,” *ICML*, pp. 720–729, 2015.

[22] O. Tuzel, F. Porikli, and P. Meer, “Region covariance: A fast descriptor for detection and classification,” in *ECCV*, 2006, pp. 589–600.

[23] J. Ren, X.-j. Wu, and J. Kittler, “Discriminative block-diagonal covariance descriptors for image set classification,” *Pattern Recognition Letters*, vol. 136, pp. 230–236, 2020.

[24] V. Arsigny, P. Fillard, X. Pennec, and N. Ayache, “Log-euclidean metrics for fast and simple calculus on diffusion tensors,” *Magn. Reson. Med.*, vol. 56, no. 2, pp. 411–421, 2006.

[25] B. Kulis, M. Sustik, and I. Dhillon, “Learning low-rank kernel matrices,” *ICML*, pp. 505–512, 2006.

[26] X. Pennec, P. Fillard, and N. Ayache, “A riemannian framework for tensor computing,” *IJCV*, vol. 66, no. 1, pp. 41–66, 2006.

[27] S. Sra, “A new metric on the manifold of kernel matrices with application to matrix geometric means,” *NIPS*, vol. 25, pp. 144–152, 2012.

[28] D. B. Thiyam, S. Cruces, J. Olias, and A. Cichocki, “Optimization of alpha-beta log-det divergences and their application in the spatial filtering of two class motor imagery movements,” *Entropy*, vol. 19, no. 3, p. 89, 2017.

[29] R. Wang, X.-J. Wu, K.-X. Chen, and J. Kittler, “Multiple riemannian manifold-valued descriptors based image set classification with multi-kernel metric learning,” *IEEE-TBD*, 2020.

[30] M. T. Harandi, C. Sanderson, R. Hartley, and B. C. Lovell, “Sparse coding and dictionary learning for symmetric positive definite matrices: A kernel approach,” *ECCV*, pp. 216–229, 2012.

[31] Y. LeCun, L. Bottou, Y. Bengio, and P. Haffner, “Gradient-based learning applied to document recognition,” *Proceedings of the IEEE*, vol. 86, no. 11, pp. 2278–2324, 1998.

[32] A. Krizhevsky, I. Sutskever, and G. E. Hinton, “Imagenet classification with deep convolutional neural networks,” *NIPS*, vol. 25, pp. 1097–1105, 2012.

[33] Z. Huang and L. V. Gool, “A riemannian network for spd matrix learning,” *AAAI*, pp. 2036–2042, 2017.

[34] T. Zhang, W. Zheng, Z. Cui, Y. Zong, C. Li, X. Zhou, and J. Yang, “Deep manifold-to-manifold transforming network for skeleton-based action recognition,” *IEEE-TMM*, vol. 22, no. 11, pp. 2926–2937, 2020.

[35] R. Wang, X.-J. Wu, and J. Kittler, “Symnet: A simple symmetric positive definite manifold deep learning method for image set classification,” *IEEE-TNNLS*, pp. 1–15, 2021.

[36] D. Brooks, O. Schwander, F. Barbaresco, J.-Y. Schneider, and M. Cord, “Riemannian batch normalization for spd neural networks,” *NIPS*, 2019.

[37] S. Belongie, J. Malik, and J. Puzicha, “Shape matching and object recognition using shape contexts,” *IEEE-TPAMI*, vol. 24, no. 4, pp. 509–522, 2002.

[38] D. G. Lowe, “Distinctive image features from scale-invariant keypoints,” *IJCV*, vol. 60, no. 2, pp. 91–110, 2004.

[39] C. Szegedy, W. Liu, Y. Jia, P. Sermanet, S. Reed, D. Anguelov, D. Erhan, V. Vanhoucke, and A. Rabinovich, “Going deeper with convolutions,” in *CVPR*, 2015, pp. 1–9.

[40] R. Chakraborty, J. Bouza, J. Manton, and B. C. Vemuri, “Manifoldnet: A deep neural network for manifold-valued data with applications,” *IEEE-TPAMI*, 2020.

[41] V. Arsigny, P. Fillard, X. Pennec, and N. Ayache, “Geometric means in a novel vector space structure on symmetric positive-definite matrices,” *SIAM journal on matrix analysis and applications*, vol. 29, no. 1, pp. 328–347, 2007.

[42] S. Awodey, *Category theory*. Oxford university press, 2010.

[43] S. Roman, S. Axler, and F. Gehring, *Advanced linear algebra*. Springer, 2005, vol. 3.

[44] S. Gao, M.-M. Cheng, K. Zhao, X.-Y. Zhang, M.-H. Yang, and P. H. Torr, “Res2net: A new multi-scale backbone architecture,” *IEEE-TPAMI*, 2019.

[45] T.-K. Kim and R. Cipolla, “Canonical correlation analysis of video volume tensors for action categorization and detection,” *IEEE-TPAMI*, vol. 31, no. 8, pp. 1415–1428, 2008.

[46] K. Soomro, A. R. Zamir, and M. Shah, “Ucf101: A dataset of 101 human actions classes from videos in the wild,” *arXiv preprint arXiv:1212.0402*, 2012.

[47] G. Garcia-Hernando, S. Yuan, S. Baek, and T.-K. Kim, “First-person hand action benchmark with rgb-d videos and 3d hand pose annotations,” *CVPR*, pp. 409–419, 2018.

[48] Z. Huang, J. Wu, and L. V. Gool, “Building deep networks on grassmann manifolds,” *AAAI*, pp. 3279–3286, 2018.

[49] Z. Huang, R. Wang, S. Shan, and X. Chen, “Projection metric learning on grassmann manifold with application to video based face recognition,” *CVPR*, pp. 140–149, 2015.

[50] R. Vemulapalli, F. Arrate, and R. Chellappa, “Human action recognition by representing 3d skeletons as points in a lie group,” *CVPR*, pp. 588–595, 2014.

[51] Y. Du, W. Wang, and L. Wang, “Hierarchical recurrent neural network for skeleton based action recognition,” *CVPR*, pp. 1110–1118, 2015.

[52] J.-F. Hu, W.-S. Zheng, J. Lai, and J. Zhang, “Jointly learning heterogeneous features for rgb-d activity recognition,” *CVPR*, pp. 5344–5352, 2015.

[53] C. Feichtenhofer, A. Pinz, and A. Zisserman, “Convolutional two-stream network fusion for video action recognition,” *CVPR*, pp. 1933–1941, 2016.

[54] H. Rahmani and A. Mian, “3d action recognition from novel viewpoints,” *CVPR*, pp. 1506–1515, 2016.

[55] G. Garcia-Hernando and T.-K. Kim, “Transition forests: Learning discriminative temporal transitions for action recognition and detection,” *CVPR*, pp. 432–440, 2017.

[56] T. S. Kim and A. Reiter, “Interpretable 3d human action analysis with temporal convolutional networks,” *CVPR-W*, pp. 1623–1631, 2017.

[57] B. Tekin, F. Bogo, and M. Pollefeys, “H+o: Unified egocentric recognition of 3d hand-object poses and interactions,” *CVPR*, pp. 4511–4520, 2019.

[58] H. Liu, K. Simonyan, and Y. Yang, “Darts: Differentiable architecture search,” *ICLR*, 2018.

[59] X. Chu, T. Zhou, B. Zhang, and J. Li, “Fair darts: Eliminating unfair advantages in differentiable architecture search,” in *ECCV*, 2020, pp. 465–480.

[60] R. S. Sukthanker, Z. Huang, S. Kumar, E. G. Endsjo, Y. Wu, and L. Van Gool, “Neural architecture search of spd manifold networks,” *IJCAI*, 2021.

[61] K.-X. Chen, J.-Y. Ren, X.-J. Wu, and J. Kittler, “Covariance descriptors on a gaussian manifold and their application to image set classification,” *PR*, vol. 107, p. 107463, 2020.